Study of MHD mode and cooling process during disruptions triggered by impurities injection in J-TEXT

Y. Huang[1], Z. Y. Chen[1,2,*], Qiming Hu[1,*,a], Q.Yu[3], Z.H.Jiang[1], Y N Wei[1], Pengjuan Su[1], Chengshuo Shen[1], Daojing Guo[1], Z.J.Yang[1], X.M.Pan[1] , Mingxiang Huang[1],Qinxue Cai[1],Tong Wang[1], Z. F. Lin[1], R. H. Tong[1], W. Yan[1], Z.P.Chen[1], Y. H. Ding[1], Y. Liang[1] and J-TEXT Team

[1]*International Joint Research Laboratory of Magnetic Confinement Fusion and Plasma Physics, State Key Laboratory of Advanced Electromagnetic Engineering and Technology, School of Electrical and Electronic Engineering, Huazhong University of Science and Technology, Wuhan, 430074, China*

[2] *Chengdu University, 610106,Chengdu, China*

[3] *Max-Planck-Institut für Plasmaphysik, 85748, Garching, Germany*

*Corresponding author: Z.Y.Chen and Qiming Hu E-mail: zychen@hust.edu.cn and qhu@pppl.gov

Abstract:

The injection of a large amount of impurities is one of the possible ways for disruption mitigation on large-scale tokamaks. The deposition of impurities at the center of the plasma is the key for the radiation of plasma energy and runaway suppression. The interaction of the gas jet with the rational surfaces has been studied by scanning the plasma current. Experimental results show that the injection of a massive amount of argon can cool the plasma from edge to core region, and the cooling process is accompanied by different magnetohydrodynamic (MHD) modes when the gas jet reaches the corresponding rational surfaces. It is observed that with different edge safety factors and electron density, gas injection can induce different poloidal modes at first. Then the poloidal mode will traverse to lower m (m is the poloidal mode number) MHD activities until a 2/1 mode is initiated and a thermal quench (TQ) started. The experimental results show that the penetration of a gas jet across the rational surfaces is faster in the plasmas with pre-existing large 2/1 tearing modes, which indicates that the 2/1 mode plays an important role in the penetration process. Disruptions triggered by supersonic molecular beam injection (SMBI) display a slower cooling process compared with MGI, which can be divided into four stages. The dominant poloidal mode transition from m=3 to m=2 is associated with electron temperature recovery.

Keyword: disruption, massive gas injection, magnetic perturbation, tokamak

[a] Current address: Princeton Plasma Physics Laboratory, Princeton NJ 08543-0451, USA

1. Introduction

Plasma disruption in a tokamak is the sudden loss of magnetic confinement, i.e., a rapid, complete loss of the plasma thermal and magnetic energy [1-3]. Disruption mitigation system (DMS) is required in fusion reactors, since a disruption in large device can cause intolerable damage[4]. Massive gas injection (MGI), a disruption mitigation method, is used to reduce electromagnetic forces, radiate the plasma energy, and suppress the generation of runaway electrons (REs). Most MGI experiments have one or more fast-opening valve to deliver a massive amount of gas into plasmas. MGI has been successfully used as a rapid shutdown method in tokamaks [4].

Plasma performance after MGI is quite complex [5-11]. After the valve opens and the gas reaches the plasma edge, impurities diffuse into plasma, MHD activities are destabilized, growing tearing modes lead to a thermal quench (TQ) and the beginning of a current quench (CQ)[12]. Recent research has shown that the 2/1 mode plays an important role in plasma cooling and impurity mixing with the hot plasma [12, 13]. There may be also other islands such as m/n = 5/3 and m/n = 3/2 islands existing before a major disruption[14] (where m and n are the poloidal and toroidal mode numbers).

Both numerical simulation and experiments show that species of impurities, working pressure of MGI valve, and the q-profile have an important impact on the efficiency of disruption mitigation. Impurity mixing and radiation will change the MHD activity and vice versa[3, 5, 13, 15]. Numerical investigation for C-Mod has shown that a thermal quench is triggered even at very shallow penetration[16]. Simulations for DIII-D plasmas reveal that the phase relationship between the tearing mode and the impurity location can affect both radiation peaking factor and impurity mixing, and it also suggested that a 1/1 mode can result in asymmetrically radiated power[17]. Simulation with JOREK shows that in MGI triggered disruption, the O-point of magnetic island excited by MGI are located at the gas deposition position. The MGI causes the growth of magnetic island (m/n=2/1 and 3/2 mainly) and 1/1 internal kink mode[18]. The 3/2 island grows when a 2/1 island gets larger, since the 2/1 tearing mode steeps the current profile inside q=3/2 surface [18, 19].

For understanding the process of impurity penetration, extensive experiments have been carried out on J-TEXT tokamak, to scan over the amount of gas injection, edge safety factor, and line-average electron density. It was observed that different MHD modes was destabilized with different experimental parameters. The experimental results are given in section 2. Finally, a summary is presented in section 3.

2. Experimental results on the penetration of gas jet

2.1 Experimental setup

The Joint Texas Experimental Tokamak (J-TEXT) is the former TEXT tokamak (operating in the University of Texas at Austin in 1980's) reconstructed and renamed in Wuhan[20]. It is a conventional iron core and circular cross-section tokamak with a major radius of R_0=1.05 m and a minor radius of r = 0.25~0.27 m with a movable limiter [21]. The maximum toroidal magnetic field is B_T = 2.5 T. The maximum plasma

current is I_P = 240 kA with a 600 ms pulse length. The line average electron density is in the range of n_e=(0.5~7)×10^{19} m^{-3} and electron temperature T_e~1 keV [22].

There are two poloidal arrays of 2D Mirnov coils and one array of 24-coils (arranged in a circular shape) for the detection of MHD activities [20, 23]. The electron cyclotron emission (ECE) diagnostic system consists of a 16-channel heterodyne electron cyclotron emission detecting unit and a new 8-channel W-band detecting unit, which covers a large portion of the plasma and has a temporal resolution of 2 μs and a spatial resolution less than 1.5 cm[24, 25]. The fast framing camera which has 22k frame rate with 604×480 pixel resolution has been developed to observe the penetration of an impurity gas jet on J-TEXT [26].

Two MGI valves have been developed for J-TEXT tokamak. A 30 ml MGI valve is installed at a bottom port. It works in the range of 5-30 bar and the reaction time is about 0.3 ms[27]. As soon as the MGI valve opens, high-pressure gas can be injected into the plasma at sound speed. A supersonic molecular beam injection (SMBI) system has also been developed in J-TEXT tokamak. The number of particles in the SMBI is linearly proportional to the product of gas pressure and pulse duration[28]. The SMBI system can inject less amounts of particles than the MGI does. For the reason that large scale of argon injected to plasma will trigger a very fast cooling process in less than 1ms, it will be very difficult for diagnosing any useful signal. Moderate injection of argon atom was chosen to slow down the cooling process for measurement feasibility.

2.2 Time evolution of plasma performance after argon MGI

A typical result of MHD triggered by MGI is displayed in Figure 1. The plasma parameters of discharge #1049676 are: plasma current I_P = 105 kA, toroidal field B_T = 2.14 T, edge safety factor q_a = 6.3, and the central line-average electron density n_e~1.5×10^{19} m^{-3}. The MGI is triggered at 0.4 s. The injected argon atoms are about 2.6×10^{19}. The argon gas cooled down the plasma core with about 3 ms delay. The injection of argon initiates a magnetic perturbation within ~ 2 ms after MGI is triggered. There are some oscillations on ECE signal at r = -0.53 cm (high field side) which show that the cooling process is nonlinear. The signal of plasma current shows there is a runaway current plateau lasting about 6 ms. Analysis of the Mirnov coil array and the ECE diagnostic system in Figure 2 shows the detailed evolution of the MHD activities and cooling process of this discharge after the MGI is triggered. Since the amplitude of magnetic perturbation is small in the beginning, we choose normalized amplitude to study the MHD activities.

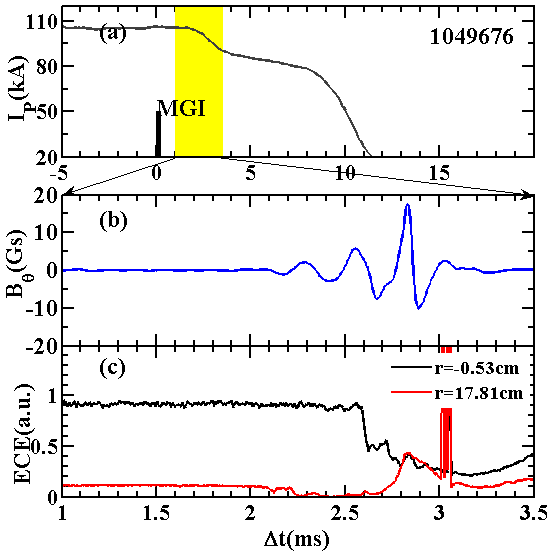

Figure 1. Time evolution of (a) plasma current, (b) poloidal magnetic perturbation, (c) ECE signals at two different radial locations for shot 1049676. The red spikes in (c) are invalid because the optical thickness condition for the ECE's measurement is not satisfied. The shadow area in (a) is described in detail in (b) and (c). The times on the figure refer to the beginning time of MGI.

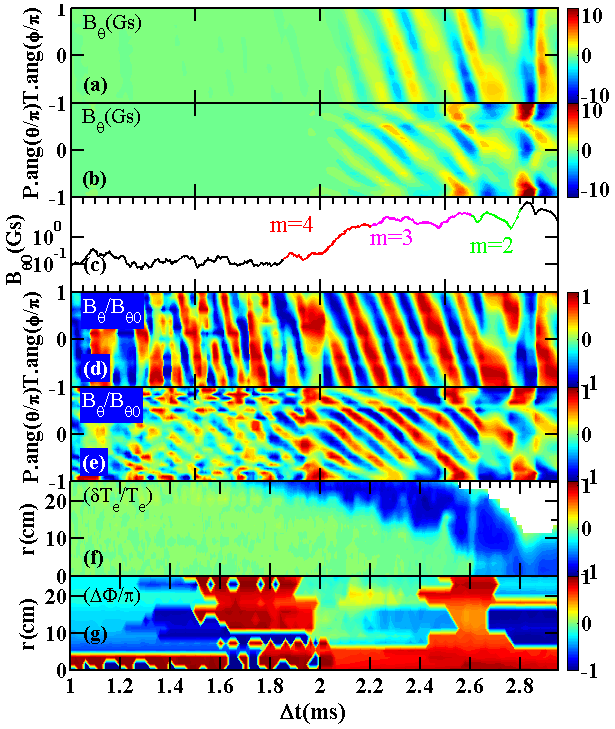

Figure 2. (a) poloidal magnetic perturbation from toroidal Mirnov array, (b) poloidal magnetic perturbation from poloidal Mirnov array, (c) maximum value of poloidal magnetic perturbation. Red, magenta and green lines in frame (c) correspond to times when the poloidal mode number equals 4, 3 and 2, respectively. (d) normalized poloidal magnetic perturbation from toroidal Mirnov array, (e) normalized poloidal magnetic perturbation from poloidal Mirnov array, (f) time evolution of electron temperature at different minor radii for shot 1049676. T_e at different positions is the average value measured from each channel of the ECE from Δt=-0.1 ms to Δt=0 ms, δT_e is the instantaneous temperature variation with respect to T_e. $\delta T_e/T_e$ describes the relative

change of electron temperature. The times on the figure refer to the beginning time of MGI. White area in (f) after 2.4ms is invalid because the optical thickness condition for the ECE's measurement is not satisfied. (g) is the phase difference between ECE signals and one channel Mirnov signal.

Figure 2 (a) and (b) show that after gas injection, the magnetic perturbation grows a short time later. Before MGI triggering, the amplitude of magnetic perturbation is tiny and no big island is presented in the plasma. Magnetic perturbations triggered by the impurity injection grow non-linearly as the cooling front enters plasma as seen from Figure 2(c). Figure 2 (d) and (f) show that the first MHD mode induced by massive argon is a m/n = 4/1 mode. With deeper plasma cooling, m/n = 3/1 and m/n = 2/1 modes appear in succession, which suggests impurity deposition at corresponding rational surfaces. The ECE diagnostic system, which covers almost the entire low field side at B_T=2.14 T, shows that plasma cooling has two processes: diffusive cooling and oscillating cooling.

The massive injected gas cools down the plasma from edge towards the central region as time involves, resulting in plasma current shrinkage and peaking [19]. This can temporally lead to a larger plasma current density gradient inside a resonant surface with $q=m/n$ but a smaller one outside the surface, and the (m, n) tearing mode can be destabilized. In addition, the shrinking current leads to the decrease of the effective edge q, the q value at edge of the plasma current channel [29]. External kink type mode might be destabilized when the effective edge q decreases a little lower than m/n [22, 29]. The phase difference between ECE signals and one channel Mirnov signal plotted in Figure 2(g), obtained by correlation analysis, shows that the m=4 MHD activity is a kink type mode or a too small island to be measured. While the later m=3 and 2 activities are tearing modes according to the phase inversion, and these tearing modes causes observable temperature perturbations, namely oscillating cooling. The high-m modes (m =6, 5 and 4) usually grow up only to low amplitude and survive only for a short period of time, and this stage behaves as diffusive cooling process. At the end of the cooling process, the measurement of $\delta T_e/T_e$ in the white area is invalid because the optical thickness condition for the ECE's measurement is not satisfied.

Figure 3 shows four photos during the penetration of the gas jet before TQ onset. When the injection of argon atoms reached the plasma boundary, there were strong emissions observed by fast frame camera with a band-pass filter of a central wavelength 442.6 nm. From the fast camera picture sequence, it is clear that the impurities spread preferentially towards the high-field side. Just before the TQ (~ 2.8 ms after MGI triggering), the dark area shows that impurities are not totally spread into plasma at this time.

To find out the dependence of MHD activity (triggered by MGI) on the edge safety factor q_a, four discharges with different q_a are presented in Figure 4. The plasma current of these four shots are: (a) 104 kA, (b) 120 kA, (c) 151 kA, (d) 195 kA, respectively. The corresponding edge safety factors are about: (a) 6.3, (b) 5.5, (c) 4.5, and (d) 3.4, respectively. The line-average electron density is about 1.7×10^{19} m^{-3} in

these shots. The number of argon atoms injected in each shot is about 2.1×10^{19}. Figure 4(a1), (b1), (c1) and (d1) show almost the same increase in the magnetic perturbation. With different edge safety factors, the MGI initially triggers a different MHD mode. As the edge safety factor decreases, the poloidal number of the first MHD activity decreases as well. The MHD modes around the outmost rational surface are not visible in figure, perhaps because they are too weak to be distinguished with Mirnov coils. The time delay between impurity reaching the edge and the collapse of core electron temperature is very similar in these shots. If $q_a \sim 3$, the 2/1 island appears first, and cooling from the r ~ 15 cm to r ~ 0 cm occurs simultaneously. The spatial resolution of ECE is about 1.8 cm in these experiments, and we have not observed the temperature flattening from neighboring 3 channels, so that the 2/1island width should be around 1.8-3.6 cm or smaller. This indicates that the 2/1 mode has an important influence on plasma cooling.

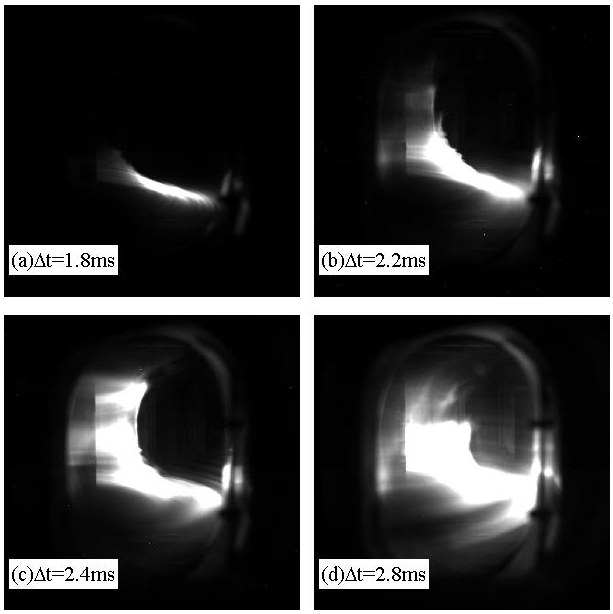

Figure 3. Observation of the penetration of the gas jet followed by disruption by a fast frame camera with a filter for shot 1049676. The times on the images refer to the beginning time of MGI. Each image's left side is the high-field side. At Δt =2.8ms the core of plasma is cooled.

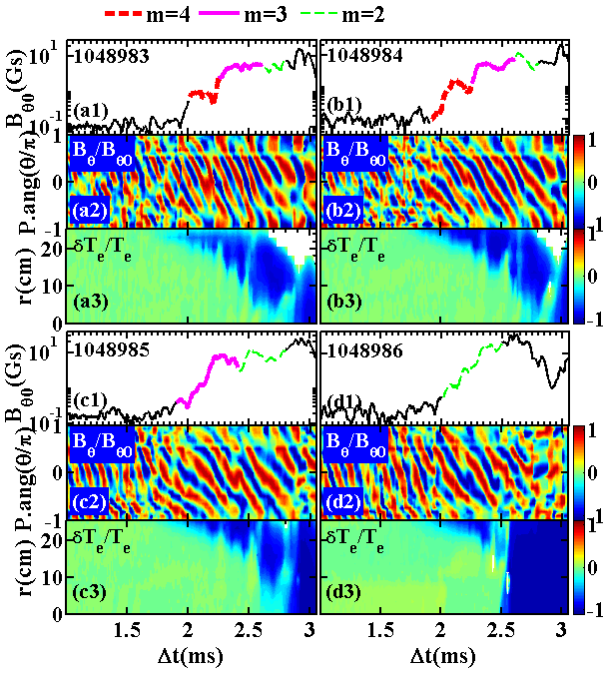

Figure 4. Time evolution of MHD instability and thermal quench with (a) q_a=6.3, (b) q_a=5.5, (c) q_a=4.5 (d) q_a=3.4 for shots 1048983, 1048984, 1048985 and 1048986, respectively. Time traces of (a1) ~ (d1) are the magnetic perturbation amplitudes; (a2) ~ (d2) are the normalized poloidal magnetic perturbations; (a3) ~ (d3) are δTe/Te from ECE signals. The times on the figure refer to the beginning time of MGI. Red, magenta and green marks in (a1), (b1), (c1) and (d1) indicate poloidal mode. White area in (a3) and (b3) are invalid because the optical thickness condition for the ECE's measurement is not satisfied.

The effect of electron density on the MHD activities induced by MGI has also been studied. Two discharges were carried out with different electron density, while about 2.1×10^{19} argon atoms were injected through the MGI valve at 0.4 s. Figure 5 shows that the electron density before the MGI has an impact on induced MHD activities. The discharge with lower electron density (shot 1048977) has a higher poloidal mode number after the MGI. In Figure 5(b2), for shot 1048998 with a higher density, the MHD mode resulting from the MGI is a 2/1 tearing mode, it grows very quickly compared to that in shot 1048977 shown by Figure 5(a2). Cooling processes are quite different in these two shots. Cooling from edge to core in shot 1048998 is much faster than that in shot 1048977, and this can be attributed to the onset of the m/n = 2/1 MHD mode at the beginning. It is worth mentioning that the 2/1 mode triggered by MGI at high electron density in Figure 5(b1) has the fastest growth rate, even faster than that at lower q_a discharge shown in Figure 4(d1). For Ohmic discharges, the injected impurity due to MGI increases plasma radiation and may cause radiation limit[30-32]. As a result, MGI may lower the Greenwald density limit and accelerate the excitation of precursor MHD, so that the 2/1 mode is excited earlier and grows up faster.

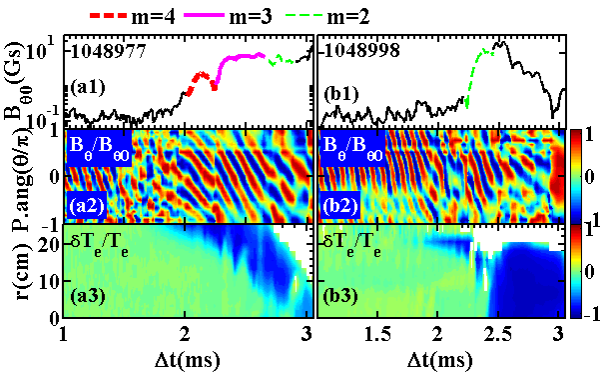

Figure 5. Poloidal magnetic perturbation and thermal quench with (a) n_e=1.3×10^{19}m^{-3}, (b) n_e=2.8×10^{19}m^{-3} for shots 1048977 and 1048998, respectfully. The edge safety factors are 5.5 for both cases. The times on the figure refer to the beginning time of MGI. White area in (a3) and (b3) are invalid because the optical thickness condition for the ECE's measurement is not satisfied.

Figure 6 and Figure 7 show the relationship of MHD modes triggered by MGI with edge safety factor, electron density and amounts of injected argon atoms. Due to the fact that the toroidal mode number equals 1 in all cases, only poloidal mode numbers are presented. It can be seen that the value of m may get close to the value of the safety factor of the outer most rational surface when the central line-averaged electron density is about 1×10^{19} m^{-3}. The electron temperature is lower in higher electron density Ohmic discharges on J-TEXT[33]. In this case the injected gas will cause a relatively smaller further decrease in electron temperature compared to that in low density discharges. The corresponding relative change in the plasma current density profile is also smaller. This might be the reason why only low *m* mode is observed at high density discharges. The edge safety factor limits the maximum value of *m*, and *m* decreases as the electron density increases. The poloidal mode number of the initial MHD mode triggered by MGI also decreases when more argon atoms are injected into plasma. There is no evidence for the existence of a *m*/*n* =6/1 mode. Even if the 6/1 mode exists, it should be too weak to be distinguished by the Mirnov probes.

Moreover, the quantity of injected impurities increased by turning up the voltage of MGI, but the gas jet speed in vacuum increases [26]. Hence there are two variables here that may have an impact on the rate of MGI cooling the plasma, and these two are not independent.

In Figure 8 (a) the radial motion of the cooling front is shown as a function of time. The number of argon atoms of the four shots in Figure 8 spans approximately two orders of magnitude. The time delay between the edge and central electron temperature collapse decreases with the increasing number of argon atoms injected, although the time when the edge of plasma starts cooling is a little different. The magnetic perturbation amplitude is the same after the cooling front reaches the core, as shown in Figure 8 (a).

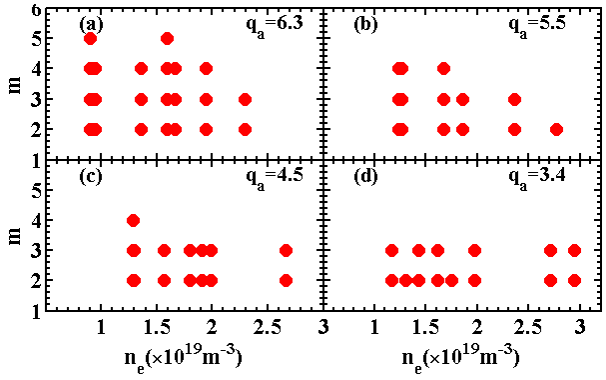

Figure 6. Dependence of poloidal mode number m on the edge safety factor and central line-average electron density. The number of argon atoms injected are about 2.1×10^{19} for all cases. Shots in each subplot have the same edge safety factor with (a) q_a=6.3, (b) q_a=5.5, (c) q_a=4.5 and (d) q_a=3.4.

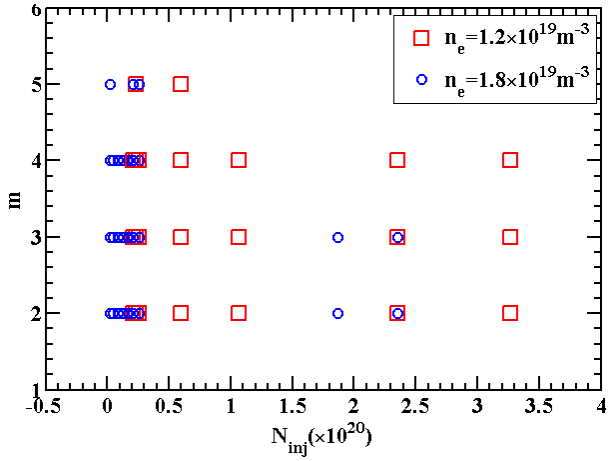

Figure 7. Dependence of poloidal mode number on the amount of Ar injected. Red squares and blue circles represent line-averaged electron densities of 1.2×10^{19}m^{-3} and 1.8×10^{19}m^{-3}, respectfully. The injected atoms are all above 10^{19}.

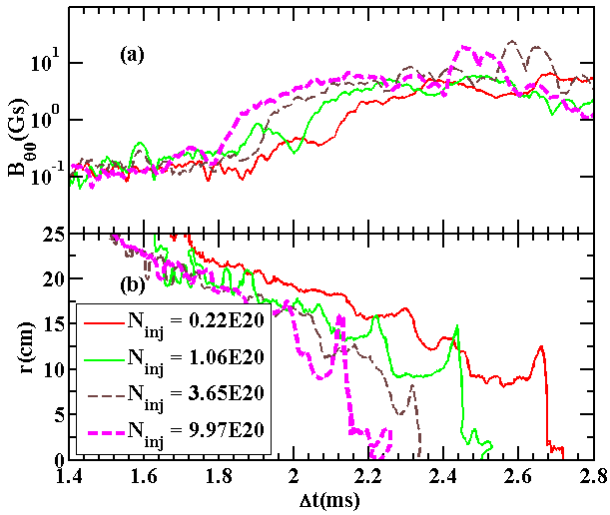

Figure 8. Dependence of magnetic perturbation and plasma cooling process on the amount of Ar injection. The different line styles represent different quantities of argon gas injection. The edge safety factors are 6.4 and the central line-average electron density are 1.5×10^{19}m^{-3}. Lines in (b) are

obtained from corresponding $\delta T_e/T_e$ contour plots, similar to that shown in figure 5, such that these lines have the same constant value of $\delta T_e/T_e$ in the coordinates (Δt-r), showing the time evolution of the same $\delta T_e/T_e$ along the minor radius. The times on the figure refer to the beginning time of MGI.

Early experiments showed that the m/n =2/1 tearing mode cooled down the plasma from edge towards core very quickly[34, 35]. To explore the effect of the 2/1 tearing mode, discharges with q_a=2.8, central line-averaged electron density about 1.2×10^{19} m^{-3} and different argon injection amounts were carried out. Figure 9 displays four shots, where the number of injected argon atoms is 2.5×10^{19}, 1.7×10^{21}, 2.5×10^{18}, 1×10^{21}, respectively. In Figure 9 (a) and (b) there is no big island before MGI triggering. The opposite situation is shown in Figure 9 (c) and (d), where a big 2/1 island is present before MGI triggering. It is clear that with such a wide range of injection, the influence of the 2/1 mode on cooling process is similar. The phase difference between ECE signals and one channel Mirnov signal in Figure 9 (c3) and (d3) show that the MHD activity before MGI triggering is a tearing mode according to the phase inversion. That phase inversion quickly changes after MGI triggering because of the fast cooling from edge to core. When there is no big island before MGI, the cooling process still lasts ~ 1.4ms even with large scale Argon injection. The cooling from edge to core of the two shots with a pre-existing 2/1 island in Figure 9 occurs at the same time. A little difference exists in the time when the edge electron temperature starts collapsing, and this might be due to the change in gas injection velocity when the MGI high voltage is changed[26].

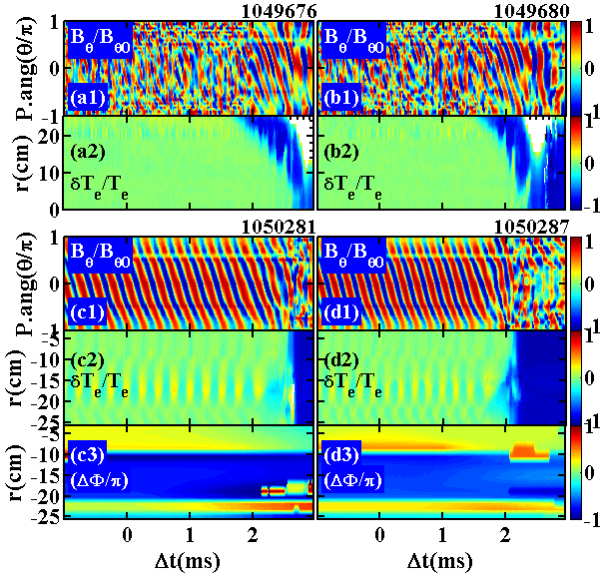

Figure 9. (a) and (b) are the time evolution of MHD instability and thermal quench when there is no big island before MGI triggering. (c) and (d) are for the cases that there is a strong 2/1 mode before MGI triggering. (c3) and (d3) are the phase difference between ECE signals and one channel Mirnov signal. The number of argon atoms is (a) 2.5×10^{19}, (b) 1.7×10^{21}, (c) 2.5×10^{18}, (d) 1×10^{21}. The times on the figure refer to the beginning time of MGI. Minus radii are in the high field side. White area in (a2) and (b2) are invalid because the optical thickness condition for the ECE's measurement is not satisfied.

2.3 Time evolution of plasma performance after massive argon gas injected by SMBI

In subsection 2.2, it has been shown that disruptions triggered by MGI with Argon injection have multiple MHD modes and a two-stage cooling process. In order to study the cooling process and associated evolution of MHD activities in more detail, SMBI (Supersonic Molecular Beam Injection) with lower gas injection rate was applied to trigger disruptions. SMBI can inject moderate argon number (injected argon number of SMBI is a function of the product of gas pressure in the valve and pulse duration) to trigger a disruption with longer duration. The SMBI argon penetration process before TQ onset is much slower than MGI.

In Figure 10 there are three shots with different pulse length of SMBI, which means different amounts of impurity have been injected into vacuum vessel. The cooling from the edge at r=20 cm starts at about 1.8 ms after the SMBI is triggered, but the start of core plasma cooling is about 4 ms after SMBI is triggered. The core of plasma has two cooling processes, which can be seen from soft X-ray emission and electron cyclotron emission in the core of plasma (first at 4 ms and next at about 6~7 ms). The time duration of cooling from edge to core with impurity injected by SMBI under these settings is slower than MGI. In addition, when the pulse length of SMBI is longer than 3 ms, there is no evidence of a different cooling process, so 2 ms as the pulse length of SMBI was set in subsequent experiments.

The MHD activities of the discharges in Figure 10 are very different from that triggered by MGI. The magnetic perturbations are decomposed using the equation $B_\theta = \sum_i A_i \times \sin(m_i\theta + \varphi + \Delta\Phi_i)$, where m is the poloidal mode number, θ and φ are the poloidal and toroidal angle, $\Delta\Phi_i$ is the phase of each modes, and A is the amplitude of the corresponding poloidal mode. In Figure 11 (a), the first mode is *m*=4, then it quickly changes to *m*=3 at ~ 3 ms. After 4 ms, the amplitudes of *m*=3 and *m*=2 modes are similar. The fast transition from *m*=4 to *m*=3 is consistent with the high speed of gas jet by SMBI (about 700m/s). The injected argon atoms per ms by SMBI is smaller than that by MGI in these experiments. And the cooling of plasma by impurity radiation is weaker than MGI experiments, leading to smaller amplitude of MHD activities triggered by SMBI. Before a totally TQ, there is a series of partial disruption and temperature recovery as shown in Figure 11 (b).

To understand why the electron temperature has a recovery in the core, 4 discharges with different edge safety factors of 6.2, 5.4, 4.3, 3.4 are shown in Figure 12. The gas pressures in the valve and pulse length of SMBI are almost the same.

The relative change of electron temperature profile in Figure 12(a) consists of four phases: from 1.5 ms to about 4 ms after SMBI was triggered (from arrow 1 to arrow 2), the cooling front transfers linearly from edge towards core. Slightly later a fast cooling from r~14 cm to r~8 cm happens (near arrow 2), and then the core electron temperature falls and electron temperature of the adjacent plasma rises. The cooling front seems to propagate backward (from arrow 2 to arrow 3), and ends with an instant cooling from r~15 cm to r~0 cm nearly arrow 3.

As mentioned before, J-TEXT is an Ohmic-heating device, so that the change of plasma current also affect the electron temperature. In order to eliminate the effects of

electron temperature, several shots with the same plasma current but different electron densities were made. In Figure 12(b), three shots are shown with edge safety factors equal to 4.3, and electron density changes from 1.5×10^{19} m^{-3} to 2.5×10^{19} m^{-3}. The cooling process seems to have little change except for the starting time of second cooling. In Figure 12(b) the time duration from electron temperature recovery (at about 4 ms) to the overall quench (at about 5 ms) resembles the previous results that high electron density has a sudden overall decline.

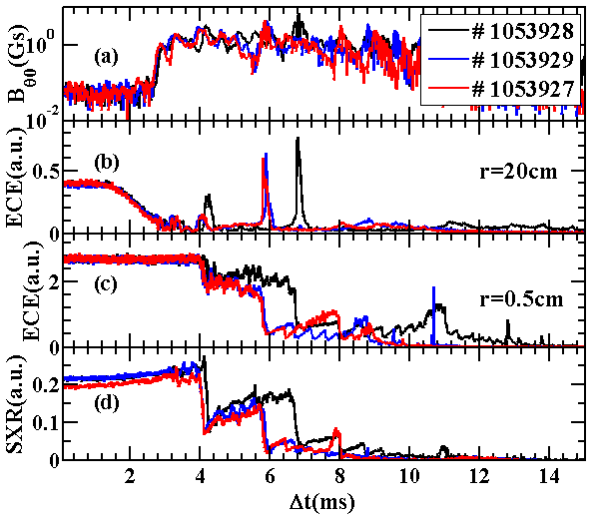

Figure 10. Three shots of different pulse length of SMBI with q_a=6.2, n_e=1.2×10^{19} m^{-3}, B_T=2.1 T. The pulse length of SMBI in shot 1053928, 1053929 and 1053927 is 2 ms, 2.5 ms, and 3 ms, respectfully. The gas pressure of the SMBI is about 1.32~1.45 MPa. Signals from top to bottom are (a)amplitude of magnetic perturbation, (b)ECE signals at r=20 cm, (c)ECE signals at r=0.5 cm and (d)soft X-ray emission in the core. The times on the figure refer to the beginning time of SMBI.

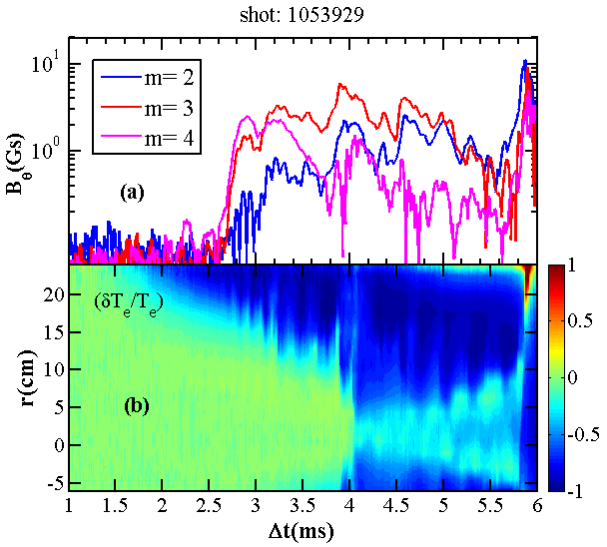

Figure 11. (a)Time evolution of amplitudes of m=4, 3 and 2. (b) Time evolution of cooling process.

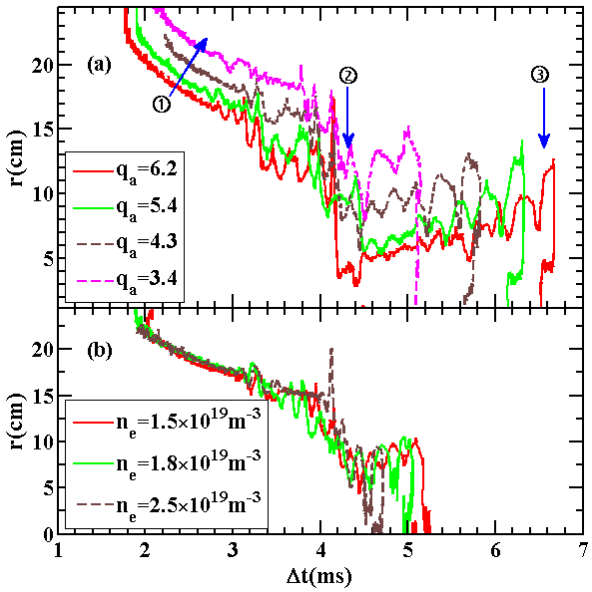

Figure 12. (a)Relationship between edge safety factor and electron temperature recovery. n_e=1.2×10^{19} m^{-3}, B_T=2.1 T for each shot here. (b)Relationship between electron density and electron temperature recovery. B_T=2.1T, q_a=4.3 for each shot here. The gas pressure of SMBI is about 1.37~1.45 MPa. The SMBI pulse length is 2 ms for all of the shots above. Lines in (a) and (b) are obtained from corresponding $\delta T_e/T_e$ contour plots such that these lines have the same constant value of $\delta T_e/T_e$ (−0.3 in (a) and −0.2 in (b)) in the coordinates (Δt-r), showing the time evolution of the same $\delta T_e/T_e$ along the minor radius. The times on the figure refer to the beginning time of SMBI.

Corresponding to Figure 12 (a), the perturbation amplitudes of m=2 and m=3 modes shown in Figure 13 reveal the evolution of poloidal modes before and after the electron temperature recovery. In shots with q_a=6.2 and q_a=5.4, the measured magnitude of m=3 modes are larger than m=2 modes at about 4 ms after SMBI is triggered. After 5 ms, the measured magnitudes of m=2 modes and m=3 modes are approximately equal. Considering that q=2 is closer to Mirnov arrays than q=3 surface, the dominant mode is m=2 after 5ms, implying the change of the dominant mode in the plasma. In other words, the magnitude of the m=2 mode is stronger compared with the m=3 mode after recovery occurs. The amplitude of the perturbation reaches its maximum value before the sudden quench. Other two cases also indicate that the m=2 mode becomes stronger in a later time.

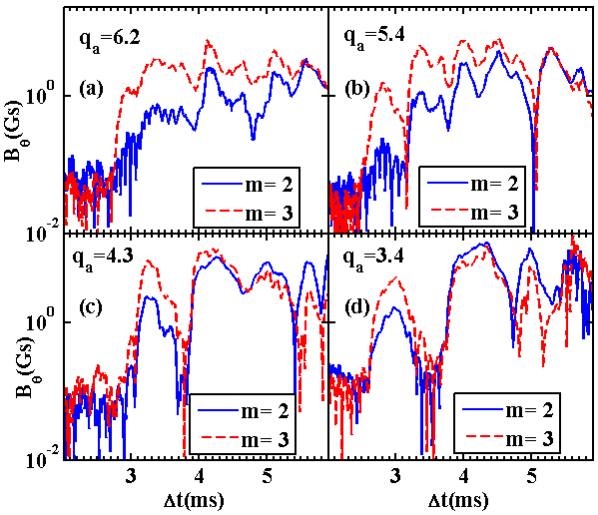

Figure 13. MHD mode amplitude of *m*=2 and *m*=3 after the SMBI is triggered. Shots presented here are the same as those in Figure 12(a). The times on the figure refer to the beginning time of SMBI.

3. Discussion and summary

In summary, the MHD modes and cooling processes during disruption triggered by MGI and SMBI have been studied in J-TEXT. The behavior of MHD activities at the time of the pre-TQ and the TQ onset was described in detail. It was found that a massive number of argon atoms injected to plasma initiates MHD activities. The data presented here give a detailed description of MHD mode evolution and cooling process during the disruption triggered by a massive argon gas injection. After the argon atoms are injected, a high-*m* MHD mode is initiated. The poloidal mode number of this mode depends on edge safety factor, line-averaged electron density, and quantity of gas injection. The edge safety factor limits the maximum value of *m*. Under lower electron density or a smaller quantity of impurity injection, the MHD modes having m values closer to the edge safety factor are destabilized. As the impurity cools the plasma deeper, the MHD mode changes to a lower-*m* mode. When the impurity injection destabilizes a 2/1 tearing mode or there is a 2/1 mode before the MGI is triggered, cooling from edge to core is very fast. In addition, we found the plasma cooling by impurity injection can be divided into two parts: diffusive cooling and oscillating cooling. The oscillating period of cooling front is similar to the MHD rotating period, which suggests that cooling may be modulated by MHD activity.

Acknowledgments

The authors are very grateful for the help of J-TEXT team and the modifications of Alan Coulter England. This work was supported by the National Natural Science Foundation of China (Nos. 11775089, 11505069, 71762031 and 11575068) and by the National Magnetic Confinement Fusion Science Program (Nos. 2015GB111001, 2015GB111002 and 2015GB104000).

Reference

[1] RICCARDO V, CONTRIBUTORS J E. Disruptions and disruption mitigation [J]. Plasma Physics and Controlled Fusion, 2003, 45(12A): A269.

[2] SCHULLER F C. Disruptions in tokamaks [J]. Plasma Physics and Controlled Fusion, 1995, 37(11A): A135.

[3] CHEN Z Y, et al. The behavior of runaway current in massive gas injection fast shutdown plasmas in J-TEXT [J]. Nuclear Fusion, 2016, 56(11): 112013.

[4] HOLLMANN E M, et al. Status of research toward the ITER disruption mitigation system [J]. Physics of Plasmas, 2015, 22(2): 021802.

[5] HOLLMANN E M, et al. Measurements of injected impurity assimilation during massive gas injection experiments in DIII-D [J]. Nuclear Fusion, 2008, 48(11): 115007.

[6] HOLLMANN E M, et al. Measurements of impurity and heat dynamics during noble gas jet-initiated fast plasma shutdown for disruption mitigation in DIII-D [J]. Nuclear Fusion, 2005, 45(9): 1046-55.

[7] TAYLOR P L, et al. Disruption mitigation studies in DIII-D [J]. Physics of Plasmas, 1999, 6(5): 1872-9.

[8] PAUTASSO G, et al. Plasma shut-down with fast impurity puff on ASDEX Upgrade [J]. Nuclear Fusion, 2007, 47(8): 900-13.

[9] LEHNEN M, et al. Disruption mitigation by massive gas injection in JET [J]. Nuclear Fusion, 2011, 51(12): 123010.

[10] THORNTON A J, et al. Characterization of disruption mitigation via massive gas injection on MAST [J]. Plasma Physics and Controlled Fusion, 2012, 54(12): 125007.

[11] WHYTE D G, et al. Disruption mitigation with high-pressure noble gas injection [J]. Journal of Nuclear Materials, 2003, 313(1239-46.

[12] IZZO V A, et al. Magnetohydrodynamic simulations of massive gas injection into Alcator C-Mod and DIII-D plasmas [J]. Physics of Plasmas, 2008, 15(5): 056109.

[13] HOLLMANN E M, et al. Observation of q-profile dependence in noble gas injection radiative shutdown times in DIII-D [J]. Physics of Plasmas, 2007, 14(1): 012502.

[14] HOPCRAFT K I, et al. Comparison of tokamak disruption simulations [J]. Nuclear Fusion, 1988, 28(7): 1265.

[15] REINKE M L, et al. Toroidally resolved radiation dynamics during a gas jet mitigated disruption on Alcator C-Mod [J]. Nuclear Fusion, 2008, 48(12): 125004.

[16] IZZO V A. A numerical investigation of the effects of impurity penetration depth on disruption mitigation by massive high-pressure gas jet [J]. Nuclear Fusion, 2006, 46(5): 541-7.

[17] IZZO V A. Impurity mixing and radiation asymmetry in massive gas injection simulations of DIII-D [J]. Physics of Plasmas, 2013, 20(5): 056107.

[18] FIL A, et al. Three-dimensional non-linear magnetohydrodynamic modeling of massive gas injection triggered disruptions in JET [J]. Physics of Plasmas, 2015, 22(6): 062509.

[19] NARDON E, et al. Progress in understanding disruptions triggered by massive gas injection via 3D non-linear MHD modelling with JOREK [J]. Plasma Physics and Controlled Fusion, 2017, 59(1): 014006.

[20] ZHUANG G, et al. The reconstruction and research progress of the TEXT-U tokamak in China [J]. Nuclear Fusion, 2011, 51(9): 094020.

[21] ZHUANG G, et al. Overview of the recent research on the J-TEXT tokamak [J]. Nuclear Fusion,

2015, 55(10): 104003.
[22] HUANG M, et al. The operation region and MHD modes on the J-TEXT tokamak [J]. Plasma Physics and Controlled Fusion, 2016, 58(12): 125002.
[23] GUO D, et al. Upgrade of the Mirnov probe arrays on the J-TEXT tokamak [J]. Review of Scientific Instruments, 2017, 88(12): 123502.
[24] YANG Z J, et al. A 16-channel heterodyne electron cyclotron emission radiometer on J-TEXT [J]. Review of Scientific Instruments, 2012, 83(10): 10E313.
[25] YANG Z J, et al. Electron cyclotron emission radiometer upgrade on the J-TEXT tokamak [J]. Review of Scientific Instruments, 2016, 87(11): 11E112.
[26] TANG Y, et al. Observation of the penetration of massive gas jet by fast frame camera on J-TEXT [J]. Physics Letters A, 2015, 379(14-15): 1043-7.
[27] LUO Y H, et al. Designing of the massive gas injection valve for the joint Texas experimental tokamak [J]. Review of Scientific Instruments, 2014, 85(8): 083504.
[28] XIAO J S, et al. A Supersonic Molecular Beam Injection System on the J-TEXT Tokamak [J]. Journal of Fusion Energy, 2015, 34(5): 1020-6.
[29] WESSON J, CAMPBELL D J. Tokamaks [M]. Oxford University Press, 2011.
[30] GIBSON A. Radiation limits to tokamak operation [J]. Nuclear Fusion, 1976, 16(3): 546.
[31] CONNOR J W, YOU S. On the density limit in tokamaks [J]. Plasma Physics and Controlled Fusion, 2002, 44(1): 121.
[32] SHI P, et al. First time observation of local current shrinkage during the MARFE behavior on the J-TEXT tokamak [J]. Nuclear Fusion, 2017, 57(11): 116052.
[33] YAN W, et al. Measurement of the electron and ion temperatures by the x-ray imaging crystal spectrometer on joint Texas experimental tokamak [J]. Review of Scientific Instruments, 2016, 87(11): 11E318.
[34] THORNTON A J, et al. Plasma profile evolution during disruption mitigation via massive gas injection on MAST [J]. Nuclear Fusion, 2012, 52(6): 063018.
[35] HENDER T C, et al. Chapter 3: MHD stability, operational limits and disruptions [J]. Nuclear Fusion, 2007, 47(6): S128.